

Supporting Information

Ni/Fe layered double hydroxide nanosheet/G-quadruplex as a new complex DNzyme with highly enhanced peroxidase-mimic activity

Yao Yao^a, Mingliang Xue^a, Wei Mao^a, Yana Li^a, Anni, Zhu^a, Tianyu Chen^a, Wei Shen^{a,*}, Chang Liu^{b*}, Lizhuang Chen^a, Sheng Tang^{a,*}

^aSchool of Environmental and Chemical Engineering, Jiangsu University of Science and Technology, Zhenjiang 212003, Jiangsu Province, PR China

^bSchool of Grain Science and Technology, Jiangsu University of Science and Technology, Zhenjiang 212003, Jiangsu Province, PR China

Corresponding authors' emails: shenweivv@126.com (W. Shen); liuchang01890@just.edu.cn (C. Liu); tangsheng.nju@gmail.com (S. Tang)

1. Experimental section

1.1 Materials

Oligonucleotides Cu-Enz (5'-/5Biotin/GGTAAGCCTGGGCCTCTTTCTTTTAAAGAAGAAC-3'), Cu-Sub (5'-/5Biotin/AGCTTCTTTCTAATACGCTTACC(A)₁₀GTGGGTCATTGTGGGTGGGTGTGG-3') were synthesized by Sangon Biotechnology Co., Ltd. (Shanghai, China) and purified by high-performance liquid chromatography. Magneticbeads (M-300 streptavidin-coated) was bought from GeteinBiotech Co., Ltd (Nanjing, China). Potassium chloride, cobalt chloride hexahydrate, cadmium chloride hemipentahydrate, zinc chloride, calcium chloride, manganese(II) chloride tetrahydrate and lead chloride, sodium acetate anhydrous, glacial acetic acid were purchased from China National Pharmaceutical Group Corporation (Shanghai, China). Disodium phosphate dodecahydrate, sodium dihydrogen phosphate dihydrate, nickel(II) chloride hexahydrate, iron(III) chloride hexahydrate and copper(II) chloride dihydrate were bought from Rich Joint Chemical Co., Ltd (Shanghai, China). Hydrogen peroxide was obtained from Chinasun Specialty Products Co., Ltd. (Jiangsu, China). 3,3',5,5'-tetramethylbenzidine (TMB) was obtained from Energy Chemical Co., Ltd (Shanghai, China). All solutions were prepared using nuclease-free ultrapure (UP) water with an electrical resistance of 18 MΩ·cm.

1.2 Apparatus

All of the UV-vis absorbance experiments were conducted on UV-2550 UV-vis spectrophotometer (Shimazu, Japan). All pH measurements were performed with a pH-3c digital pH-meter (Shanghai Lei Ci Device Works, Shanghai, China) with a combined glass-calomel electrode. Centrifugation was performed with a Scilogex D1008 centrifuge. The composition and the valence states of materials were examined by a X-ray photoelectron spectroscopy (XPS, Thermo ESCALAB 250XI). The X-ray diffraction (XRD) spectra of both native Ni/Fe-LDH and Ni/Fe-LDH/G-quadruplex were obtained by a Bruker D8 ADVANCE Powder X-ray diffractometer (Karlsruhe, Germany). All the mixing processes were conducted on a Vortex-6 Kylin-Bell

(Qilinbeier Instrument Manufacturing Co., Ltd. Beijing, China). The stabilization of LDHs in UP suspension was processed through centrifugation at a speed of 10000 rpm for 1 min by an H1850 Table Top High-Speed Centrifuge (Changsha Xiangyi Centrifuge Instrument, Changsha, Hunan, China). Absorbing infrared Fourier-transform infrared (FT-IR) spectra were recorded using a Nicolet 380 spectrophotometer in the range of 4000-400 cm^{-1} (Thermo Fisher Scientific, Shanghai, China). Scanning electron microscopy (SEM) was conducted using a JEOL JSM-6701F SEM system (Tokyo, Japan).

1.3 Synthesis of Ni/Fe-LDHs

Three types of Ni/Fe-LDH with different Ni/Fe ratio (5:1, 4:1, 3:1) were synthesized. Here, the synthesis process of Ni/Fe (3:1) LDH was described as example. $\text{Ni}(\text{NO}_3)_2 \cdot 6\text{H}_2\text{O}$ (13.088 g, 0.045 mol) and $\text{Fe}(\text{NO}_3)_3 \cdot 9\text{H}_2\text{O}$ (6.0579 g, 0.015 mol) were dissolved in beaker, which contained 100 mL deionized water. The resulted solution was transferred into the three-neck round bottom flask. Then the pH of the solution was adjusted to 10.5 by adding 2.5 M NaOH solution dropwise. Afterwards, the mixture was stirred at 60 °C for 4 hours followed by aging in the 60 °C oven without stirring for 36 hours. Finally, the resultant slurry was separated by centrifugation, washed with UP water until the pH of new filtrate is 7, and dried at 60 °C for 48 hours. The solid Ni/Fe-LDH was ground into fine powder and stored in a desiccator at ambient temperature before use.

1.4 Detection procedure

For the Cu(II) ions detection, samples containing target Cu(II) were mixed with Cu-Enz strands and Cu-Sub strands (total volume, 30 μL) in 0.01 M phosphate buffer (110 mM K^+ , pH = 7.4) at 43 °C for 2 hours. Then streptavidin-coated MBs solution was placed into a centrifuge tube and the solvent was discarded with the help of a permanent magnet. After washings with the phosphate buffer, the MBs were added into mixture. The resultant slurry was gently shaken for 30 min at ambient temperature to ensure the completion of the interaction between biotin and streptavidin. The MBs binding with Cu-Enz strands, Cu-Sub strands and the shorter DNA fragments (containing biotin label) which released from the Cu-Sub strands were separated by a permanent magnet. Next, 0.5 mg Ni/Fe-LDH was added to the supernatant containing the G-quadruplex released from the Cu-Sub strands. The final mixture reacted in the 25 °C water bath for 1 hour. The supernatant was then separated out by centrifugation. Finally, 0.1 M NaAc/HAc buffer, 10 μL of 0.2 M TMB and 20 μL of 9.9 M H_2O_2 were added to the product, making up a total volume of 1 mL. The reaction was monitored by UV-vis spectrometer and the change in absorbance was determined at 650 nm.

1.5 Preparation of human serum samples

Digestion pretreatment of serum samples from cancer patients and healthy people was conducted: firstly, 50 μL of serum was taken into a centrifuge tube, then 0.5 mL of H_2O_2 (30 %) and 20 μL of purified HNO_3 (2 %) was added. The mixture was placed for 2 hours. Finally, phosphate buffer was added to form a 100 mL system. Then the

sample was diluted 2000 times. The final solution was placed for 1 hour for following analysis.

2. Characterization of LDHs

The XRD spectra of 3:1 Ni/Fe-LDH and 3:1 Ni/Fe-LDH/G-quadruplex were depicted in Figure S1. The diffraction peaks appeared at $2\theta=11.34^\circ$, 23.45° , 35.62° , 60.15° , 62.43° corresponding to the (003), (006), (009), (110), (113) crystallographic plane of Ni/Fe-LDH (JCPDS No.38-0419). No interlayer distance increase was observed by comparing the XRD patterns of LDH before and after mixing with G-quadruplex. These results indicated that the G-quadruplex was only adsorbed on the surface of LDH, not intercalated into LDH. Since the catalytic reaction occurred on the surface of LDH, it can be deduced that the enhancing of peroxidase-like activity of LDH probably due to the adsorption of G-quadruplex.

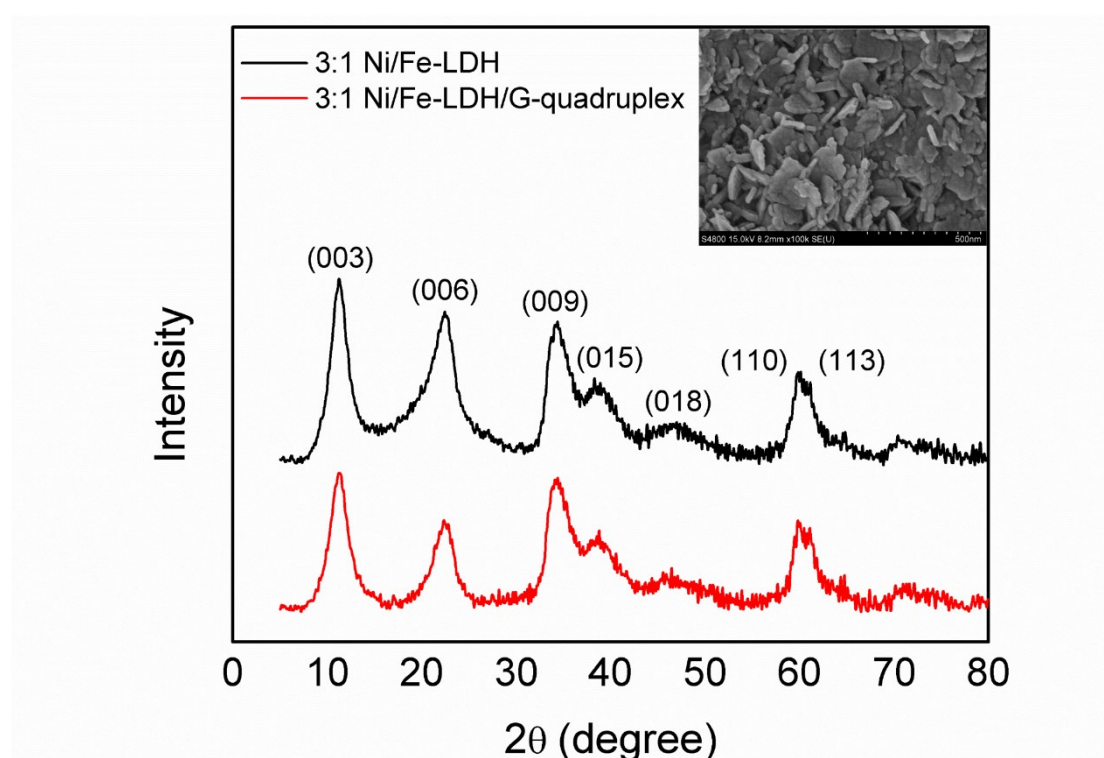


Figure S1. XRD of 3:1 Ni/Fe-LDH before and after bonded with G-quadruplex; SEM image of 3:1 Ni/Fe-LDH (insert).

To prove that the G-quadruplex has been absorbed on the surface of 3:1 Ni-Fe LDH, The SEM image of these three materials of Ni/Fe-LDH, Ni/Fe-LDH/100 nM G-quadruplex, and Ni/Fe-LDH/10 μ M G-quadruplex are investigated. As shown in Figure S2a, it can be seen that the surface of Ni/Fe-LDH is relatively smooth. Figure S2b shows the SEM of a small amount of G-quadruplex combined with Ni/Fe-LDH. Figure S2c shows the SEM of a larger number of G-quadruplex combined with Ni/Fe-LDH. It can be seen that with the increase of the concentration of G-quadruplex, the surface of complex (LDH/G-quadruplex) became more and more rough.

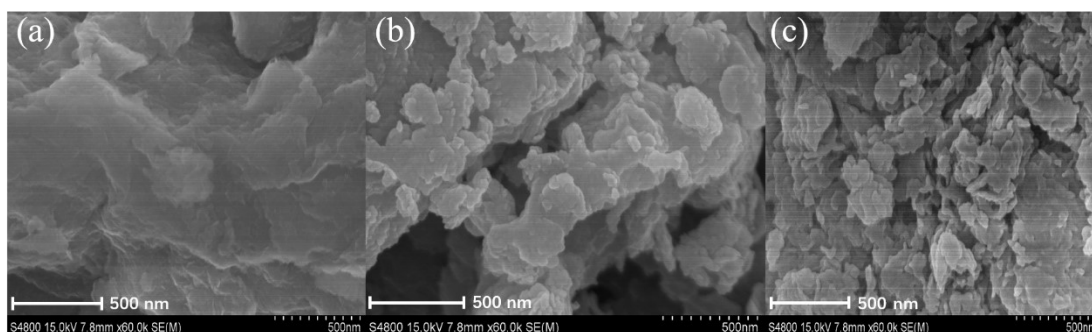


Figure S2. SEM of (a) Ni/Fe-LDH; (b) Ni/Fe-LDH/100 nM G-quadruplex; (c) Ni/Fe-LDH/10 μ M G-quadruplex.

The combination of G-quadruplex and LDH can be further proved by FT-IR spectrum, as shown in Figure S3a. The IR spectrum of Ni/Fe-LDH corresponds to that in a previous report.¹ The band at 1027 cm^{-1} of Ni/Fe-LDH/G-quadruplex coincides with the stretching vibrations of P-O bands, from G-quadruplex. The EDX and element mapping images of Ni/Fe-LDH/G-quadruplex were shown in Figure S3b and S3c, which showed that there are Ni, Fe, C, N, O, P and K elements in Ni/Fe-LDH/G-quadruplex. Ni and Fe are mainly from Ni/Fe-LDH, and P, O, and K are mainly from G-quadruplex. To further confirm the successful the binding of G-quadruplex on Ni/Fe-LDH, zeta potential of LDH, G-quadruplex and 3:1 LDH/ G-quadruplex was recorded respectively, as shown in Figure S3d. It was found that the zeta potentials of unmodified-LDH and LDH /G-quadruplex were 18.866 ± 1.266 and 8.197 ± 2.750 mV, respectively. The decreased value for LDH/G-quadruplex can be attributed to the negative charged oligonucleotide (-7.083 ± 1.414 mV). The results further indicated the successful combination of Ni/Fe-LDH and G-quadruplex.

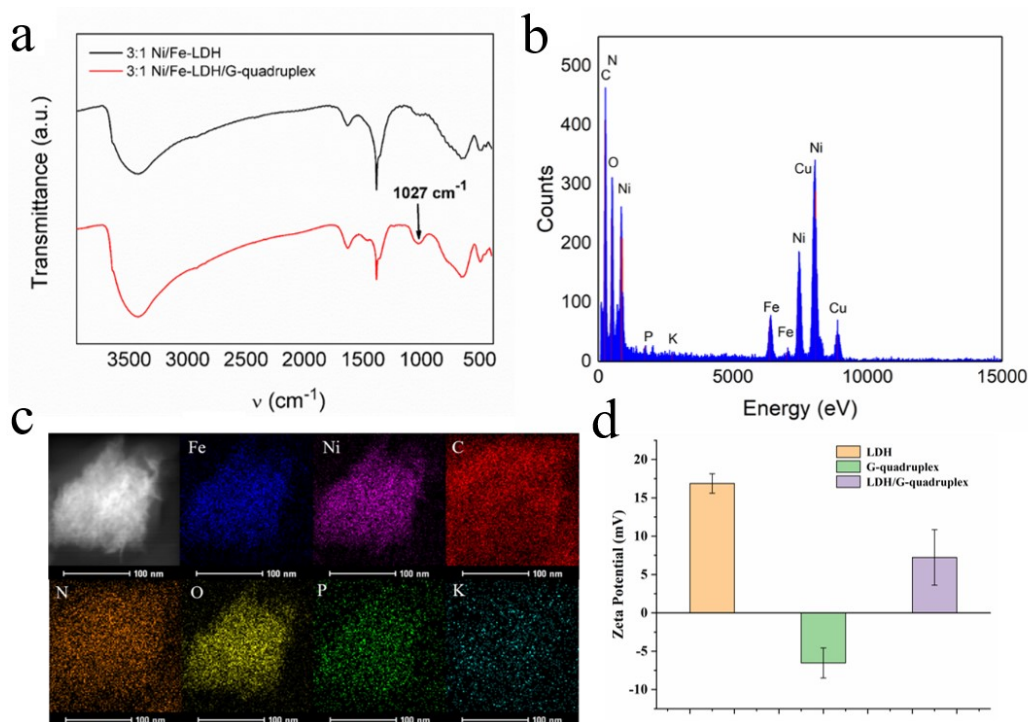


Figure S3. (a) FT-IR spectra of Ni/Fe-LDH and Ni/Fe-LDH/G-quadruplex. EDX (b) and element mapping © of Ni/Fe-LDH/G-quadruplex. (d) Zeta potential of LDH, G-quadruplex and LDH/ G-quadruplex.

3. Effect of G-quadruplex on peroxidase activity of Ni/Fe-LDH

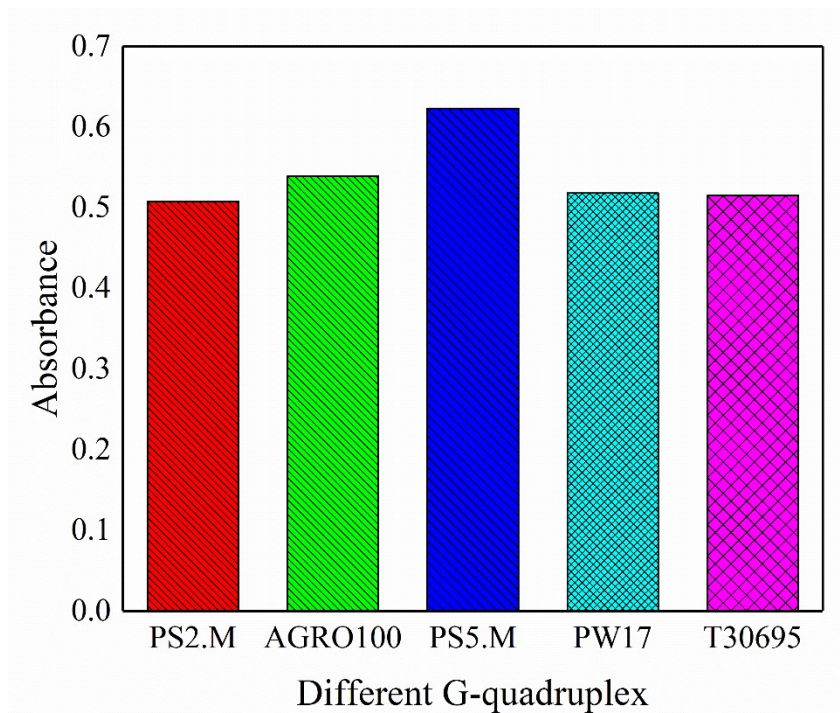


Figure S4. The catalytic activities of different types of G-quadruplexes

4. Catalytic mechanism

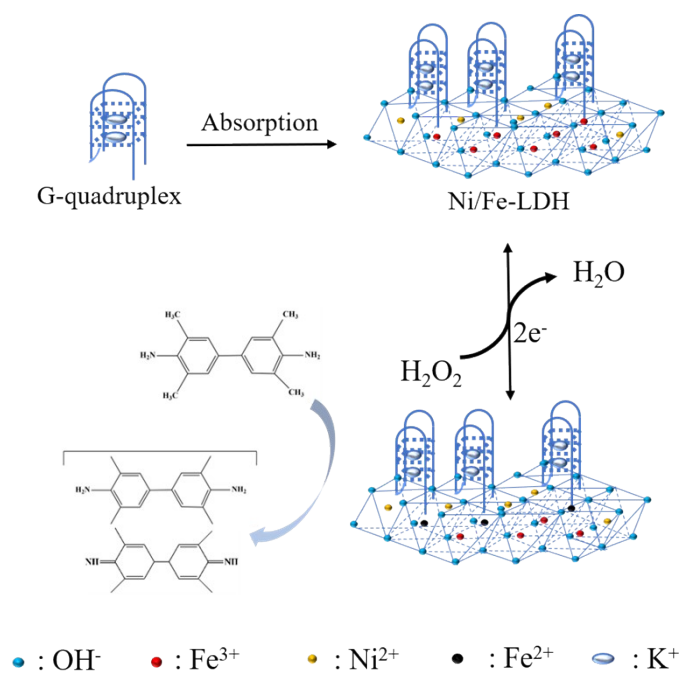


Figure S5. Illustration of the possible catalytic mechanism

5. Optimization of cleavage process

The primary analytical factor is the concentration of the Cu-Enz strands, since it is only related to the concentration of the target Cu(II).² Firstly, the target Cu(II) will enter the single-stranded DNA loop of the Cu-Enz strands. When the Cu-Sub strands and the Cu-Enz strands hybridize, the Cu-Sub strands will be cut. The concentrations of the Cu-Enz strands will affect the experimental efficiency of cleavage. When the level of the Cu-Enz strands is low, the UV-vis absorbance of final signal and the concentration of Cu(II) present a nonlinear relationship. However, if the quantity of the Cu-Enz strands is too large, it will not only increase the experiment cost, but also increase the possibility of false positive detection. Therefore, the concentration of the target Cu-Enz strands needs to be controlled suitably to achieve a higher sensitivity and lower cost. The results showed that the UV-vis absorbance increased steadily with the increasing of the Cu-Enz strands concentrations from 0.167 μM to 0.567 μM . But in the presence of higher level of the Cu-Enz strands, the UV-vis absorbance decreased (see Figure S6a). The probably reason of this phenomenon is that more target Cu(II) entered the single-stranded DNA loop of the unhybridized Cu-Enz strands. It was found that 0.567 μM Cu-Enz strands was sufficient for the following detection of Cu(II).

According to previous reports,³⁻⁵ the concentration of K^+ was essential for the formation of the DNAzyme-substrate complex and the folding of the G-quadruplex structure. Thus, the effect of K^+ on the performance of the assay was investigated. Various concentrations of K^+ were examined, and the results are plotted in Figure S6b. It can be noticed that, at a concentration of K^+ lower than 100 mM, the UV-vis absorbance was enhanced when the concentration was increased. This may be attributed to the folding efficiency of G-quadruplex and the hybridization efficiency of Cu-Enz and Cu-Sub strands enhanced at higher level of sodium, a trend found in several other DNA sensing systems.^{6,7} However, a lower UV-vis absorbance was obtained at higher K^+ concentrations (> 100 mM). The probable reason is that more K^+ entered the single-stranded DNA loop of the unhybridized Cu-Enz strands, resulting in a decrease of the Cu-Enz strands in the solution and therefore a lower UV-vis absorbance value. In consideration of the observation, 100 mM was adopted as the most favorable concentration of K^+ in the buffer.

Moreover, the hybridization efficiency, the cleavage activity and the folding efficiency can be influenced by the incubation temperature. Generally, the hybridization temperature should be 10 to 15 $^{\circ}\text{C}$ lower than the melting temperature to achieve a high hybridization efficiency and good selectivity. The estimated melting temperature of Cu-Enz was *ca.* 61 $^{\circ}\text{C}$. In principle, the assay should be performed at temperatures ≥ 46 $^{\circ}\text{C}$. However, the forming of the G-quadruplex prefers a lower temperature than 46 $^{\circ}\text{C}$.⁸ The curve in Figure S6c shows the effect of the incubation temperature, the highest absorbance was achieved at 43 $^{\circ}\text{C}$.

In addition, the incubation time of the analytical process is also an important factor. As displayed in Figure S6d, the curve flattened out after 4 hours, indicating that

the reaction was completed. However, a complete reaction was not sensitive for various concentrations of Cu(II), which limited the detection linear range. Moreover, the reaction time was too long for practical purposes. Our experiments showed that a period of 2 hours incubation is sufficient. Thus, an incubation time of 2 hours was chosen for the following experiment.

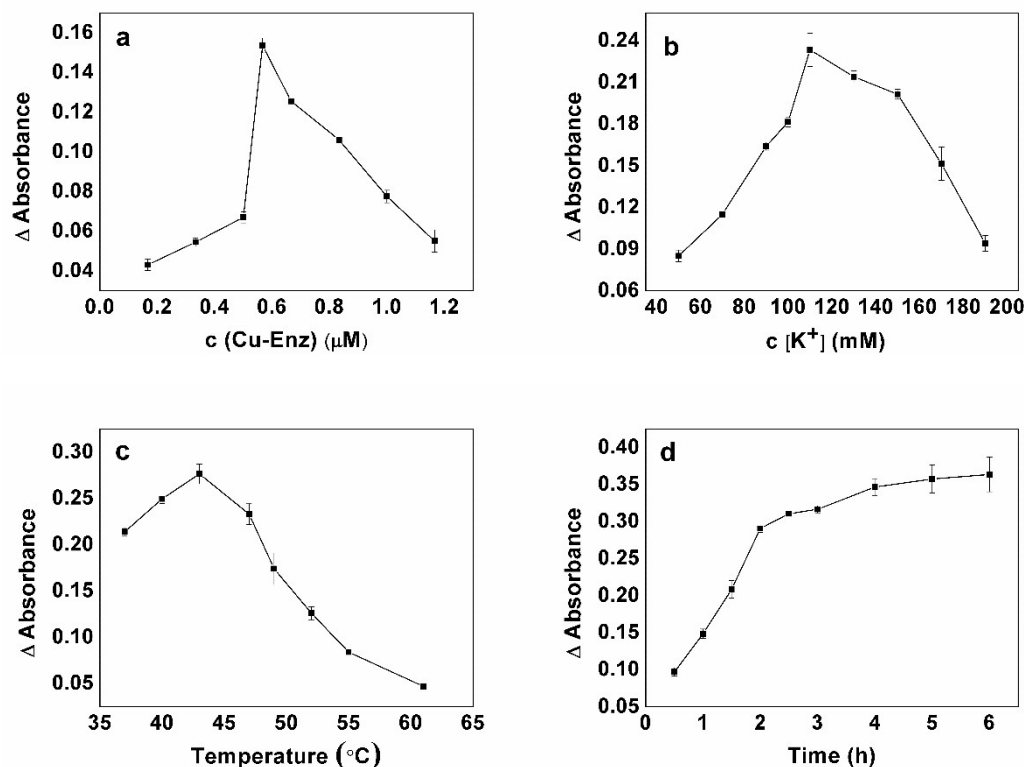


Figure S6. (a) Optimization of the concentrations of the Cu-Enz strands from 0.167 μ M to 1.167 μ M. Condition: 1 μ M Cu-Sub, 100 nM CuCl₂, pH 7.4, 90 mM K⁺, 47 $^{\circ}$ C, 2 h incubation. (b) Optimization of the concentrations of K⁺ from 50 to 190 mM in the reaction medium (0.01 M phosphate buffer). Condition: 1 μ M Cu-Sub, 0.567 μ M Cu-Enz, 100 nM CuCl₂, pH 7.4, 47 $^{\circ}$ C, 2 h incubation. (c) Optimization of the incubation temperature from 37 $^{\circ}$ C to 61 $^{\circ}$ C. Condition: 1 μ M Cu-Sub, 0.567 μ M Cu-Enz, 100 nM CuCl₂, pH 7.4, 110 mM K⁺, 2 h incubation. (d) Optimization of the incubation time from 0.5 h to 6 h. Condition: 1 μ M Cu-Sub, 0.567 μ M Cu-Enz, 100 nM CuCl₂, pH 7.4, 110 mM K⁺, 43 $^{\circ}$ C incubation.

6. Optimization of peroxidase-mimic catalytic reaction

The optimal pH value of peroxidase-mimic reaction was also processed, as shown in Figure S7. It can be seen that higher UV-vis absorbance signals were achieved at pH 4, which was also similar to the result of our previous report.⁹ In addition, the reaction rate began to slow down significantly after 7 min of reaction, and the curve became flat after *ca.* 20 min. To realize a rapid detection with low LOD and wide linear range, 7 min was adopted as the proper reaction time in this work.

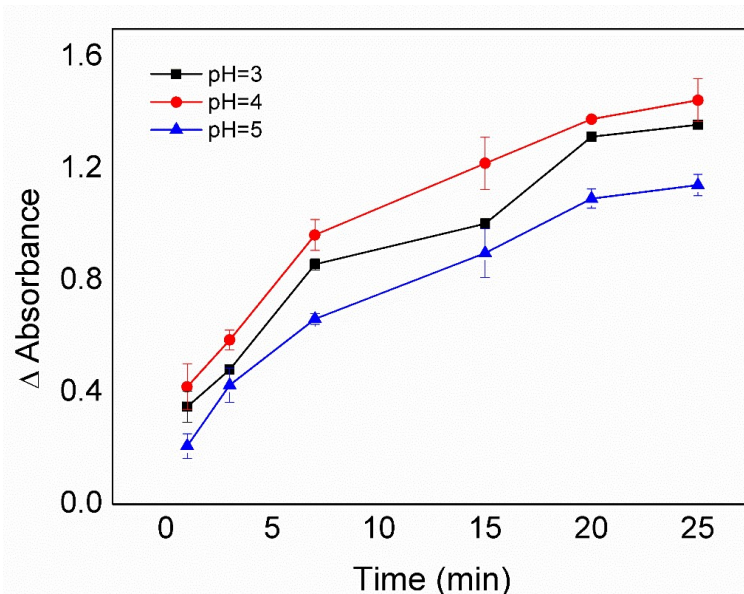


Figure S7. Effect of pH and reaction time on the TMB oxidation reaction. Conditions: 1 μM Cu-Sub, 0.567 μM Cu-Enz, 100 nM CuCl_2 , pH 7.4, 110 mM K^+ , a period of 2 h incubation at 43 $^\circ\text{C}$, 970 μL of 0.1 M NaAc/HAc buffer, 10 μL of 0.2 M TMB and 20 μL of 9.9 M H_2O_2 . Error bars show the standard deviations ($n = 3$).

7. Catalytic activity of LDH and LDH/G-quadruplex as peroxidase mimic

The apparent steady-state kinetic parameters of the H_2O_2 -mediated oxidation of TMB were calculated to evaluate the peroxidase activity of LDH and LDH/G-quadruplex, as shown in Figure S8 and Figure S9. It can be seen that the peroxidation rate increases at first and then approaches a plateau for both TMB and the H_2O_2 . The apparent Michaelis-Menten steady state kinetic parameters (K_m) could be obtained by using the Lineweaver-Burk double reciprocal plots, and the K_m value could be used to evaluate the strength of the affinity between the catalyst and the substrate (H_2O_2 and TMB). From Figure S8b and Figure S9b, it could be calculated that when considering TMB as the substrate, the K_m values of LDH and LDH/G-quadruplex were 0.527 mM and 0.174 mM, separately. From Figure S8d and Figure S9d, the K_m values of LDH and LDH/G-quadruplex were separately calculated as 0.683 mM and 0.389 mM, when H_2O_2 was chosen as the substrate. The above results indicated that LDH/G-quadruplex exhibited stronger peroxidase activity than LDH or G4/hemin ($K_m = 0.5$ mM (TMB)).¹⁰

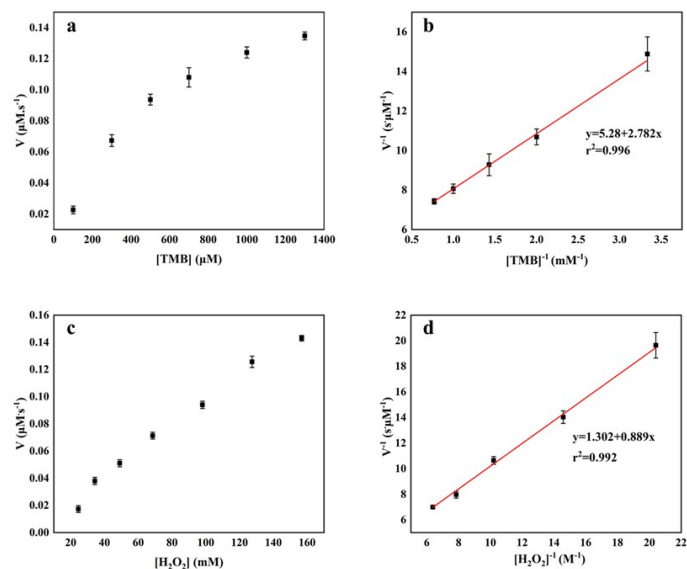


Figure S8. The initial reaction rate corresponding to the concentration of (A) TMB and (C) H_2O_2 , using $1 \text{ mg}\cdot\text{mL}^{-1}$ LDH in $970 \text{ }\mu\text{L}$ acetate buffer ($[\text{Na}^+] = 0.1 \text{ M}$, $\text{pH} = 4.0$) for 5 mins. (B) and (D) are double reciprocal plots of catalytic activity of LDH corresponding to varied concentrations of the second substrate for TMB (with $[\text{H}_2\text{O}_2] = 49 \text{ mM}$) and H_2O_2 (with $[\text{TMB}] = 500 \text{ }\mu\text{M}$), respectively.

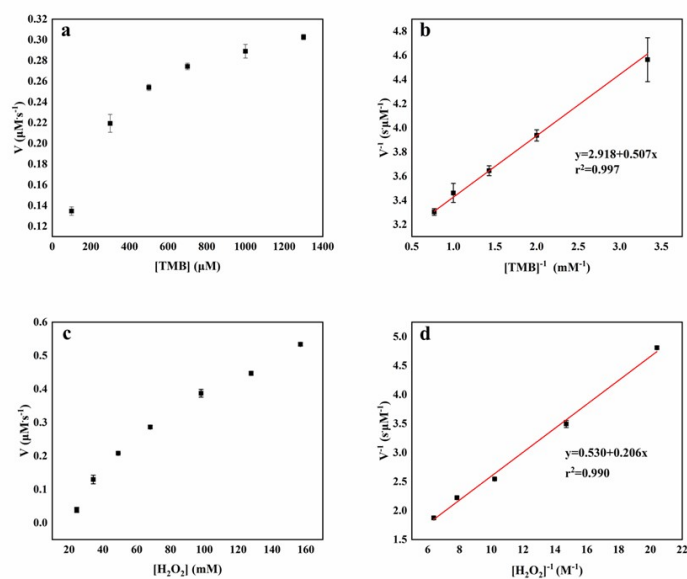


Figure S9. The initial reaction rate corresponding to the concentration of (A) TMB and (C) H_2O_2 , using $1 \text{ mg}\cdot\text{mL}^{-1}$ LDH/G-quadruplex in $970 \text{ }\mu\text{L}$ acetate buffer ($[\text{Na}^+] = 0.1 \text{ M}$, $\text{pH} = 4.0$) for 5 mins. (B) and (D) are double reciprocal plots of catalytic activity of LDH corresponding to varied concentrations of the second substrate for TMB (with $[\text{H}_2\text{O}_2] = 49 \text{ mM}$) and H_2O_2 (with $[\text{TMB}] = 500 \text{ }\mu\text{M}$), respectively.

8. Selectivity of the present assay for Cu(II)

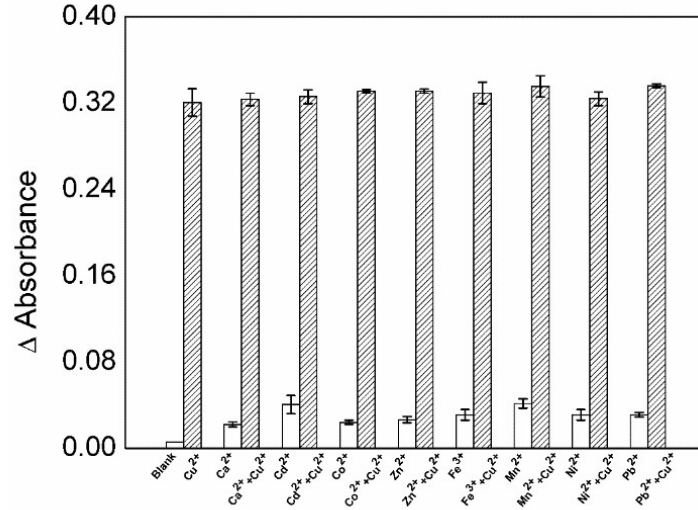


Figure S10. Responses of the sensor to various metal ions (100 nM, except Cu(II) is 1 nM) standard solution in the absence or presence of additional Cu(II) (1 nM). Condition: 1 μ M Cu-Sub, 0.567 μ M Cu-Enz, pH 7.4, 110 mM K⁺, 43 °C, 2 h incubation, catalytic reaction time 7 min, pH 4.

9. Real sample analysis and method comparison

Table S1. Determination of Cu(II) spiked in serum samples

Sample	Spiked Cu(II) (nM)	This method (RSD%, n = 3)	Relative recovery (%)	ICP-MS (RSD%, n = 3)
Healthy people Serum sample 1	Blank	7.93 (1.32)	-	7.3 (2.28)
Healthy people Serum sample 2	Blank	6.83 (4.37)	-	6.5 (1.46)
	Blank + 10	16.17 (3.47)	93.4	15.7 (3.23)
	Blank + 100	103.03 (2.58)	96.2	104.5 (2.26)
Cancer patient Serum sample 3	Blank	11.79 (1.37)	-	11.3 (2.53)
Cancer patient Serum sample 4	Blank	13.17 (3.57)	-	13.8 (1.46)
	Blank + 10	23.44 (2.55)	102.7	22.5 (3.05)
	Blank + 100	108.73 (3.75)	95.56	106.7 (2.35)

$$^a\text{Relative recovery} = (\text{Concentration}_{\text{total}} - \text{Concentration}_{\text{blank}}) / \text{Concentration}_{\text{spiked}}$$

Table S2. Comparison with other DNAzyme-based sensors for Cu(II) detection

Method	Material/indicator	Sample	LOD (pM)	Linear range (nM)
Electrochemical detection	Hemin/G-quadruplex based DNAzyme and Cu ²⁺ -specific DNAzyme	River water	0.06	0.0001 – 5 ¹¹
Fluorescence	Gold nanoparticles and Cu ²⁺ -specific DNAzyme	River water	1000	1 -10000 ¹²

	DNA cleavage-dependent graphene-quenched Cu ²⁺ -specific DNAzyme	Water	365	10 - 500 ¹³
	DNAzyme Modified Gold Nanoparticle	Living cells	450	1 - 20 ¹⁴
Colorimetric detection	Gold nanoparticles and Cu ²⁺ -specific DNAzyme	Water	60	0.1 - 2 ¹⁵
	Hemin/G-quadruplex based DNAzyme	Tap water	5900	50 - 50000 ¹⁶
	Hemin/G-quadruplex based DNAzyme and Cu ²⁺ -specific DNAzyme	Standard solution	4000	10 - 200 ¹⁷
This work	Ni/Fe-LDH/G-quadruplex based DNAzyme and Cu ²⁺ -specific DNAzyme	Serum sample	0.29	0.001 - 10000

References

- Zhan, T. R.; Kang, J. X.; Li, X. J.; Pan, L.; Li, G. J. and Hou, W. G. *Sens. Actuators B*, 2018, **255**, 2635–2642.
- Liu, J. W. and Lu, Y. *J. Am. Chem. Soc.*, 2007, **129**, 9838-9839.
- Yin, H. H.; Kuang, H.; Liu, L. Q.; Xu, L. G.; Ma, W.; Wang, L. B. and Xu, C. L. *ACS Appl. Mater. Interf.*, 2014, **6**, 4752-4757.
- He, F.; Tang, Y.; Wang, S.; Li, Y. and Zhu, D. *J. Am. Chem. Soc.*, 2005, **127**, 12343-12346.
- Li, T.; Wang, E. K. and Dong, S. *J. Chem. Commun.*, 2008, **5**, 580-582.
- Davis, J. T. *Angew. Chem. Int. Ed.*, 2004, **43**, 668-698.
- Ge, C. C.; Luo, Q.; Wang, D.; Zhao, S. M.; Liang, X. L.; Yu, L. X.; Xing, X. R. and Zeng, L. W. *Anal. Chem.*, 2014, **86**, 6387-6392.
- Wang, S. J.; Liu, C. C.; Li, G. Y.; Sheng, Y. J.; Sun, Y. S.; Rui, H. Y.; Zhang, J.; Xu, J. C. and Jiang, D. Z. *Am. Chem. Soc. Sens.*, 2017, **2**, 364-370.
- Verwilt, P.; Sunwoo, K.; Kim, J. *Chem. Commun.*, 2015, **51**, 5556-5571.
- Y. Guo, H. Wang, F. Zhang, J. Xia and Z. Wang, *Anal. Chim. Acta*, 2020, **1140**, 10-17.
- Xu, M. D.; Gao, Z. Q.; Wei, Q. H.; Chen, G. N.; Tang, D. P. *Biosens. Bioelectron.*, 2015, **74**, 1-7.
- Yin, B. C.; Zuo, P.; Huo, H.; Zhong, X. H. and Ye, B. C. *Anal. Biochem.* 2010, **401**, 47-52.
- Liu, M.; Zhao, H.; Chen, S.; Yu, H.; Zhang, Y.; Quan, X. *Biosens. Bioelectron.*, 2011, **26**, 4111-4116
- Li, L. Feng, J.; Fan, Y. Y. and Tang, B. *Anal. Chem.* 2015, **87**, 4829-4835.
- Miao, X. M.; Ling, L. S.; Du, C. G. and Shuai, X. T. *Analyst.* 2012, **137**, 3064-3069.
- Ge, C. C.; Luo, Q.; Wang, D.; Zhao, S. M.; Liang, X. L.; Yu, L. X.; Xing, X. R. and Zeng, L. W. *Anal. Chem.* 2014, **86**, 6387-6392.
- Zhang, Q.; Cai, Y.; Li, H.; Kong, D. M. and Shen, H. X. *Biosens. Bioelectron.* 2012, **38**, 331-336.